Ann. Occup. Hyg., 2014, Vol. 58, No. 5, 646–656
doi:10.1093/annhyg/meu005
Advance Access publication 6 May 2014

The Chartered Society for Worker Health Protection

Measurement of Mass-Based Carbon Nanotube Penetration through Filtering Facepiece Respirator Filtering Media

Evanly Vo[1*], Ziqing Zhuang[1], Eileen Birch[2], Qi Zhao[2], Matthew Horvatin[3] and Yuewei Liu[1]

1.National Institute for Occupational Safety and Health, National Personal Protective Technology Laboratory, 626 Cochrans Mill Road, P.O. Box 18070, Pittsburgh, PA 15236, USA;
2.National Institute for Occupational Safety and Health, Division of Applied Research and Technology, 4676 Columbia Parkway, Cincinnati, OH 45226, USA;
3.URS Corporation, 626 Cochrans Mill Road, Pittsburgh, PA 15236, USA
*Author to whom correspondence should be addressed. Tel: +1-412-386-5201; fax: +1-412-386-5250; e-mail: eav8@cdc.gov
Submitted 23 October 2013; revised 13 December 2013; revised version accepted 22 December 2013.

ABSTRACT

Recent studies suggest that a wide range of human health effects could result from exposure to carbon nanotubes (CNTs). A National Institute for Occupational Safety and Health survey of the carbonaceous nanomaterial industry found that 77% of the companies used respiratory protection, such as filtering facepiece respirators (FFRs). Despite CNT studies in some occupational settings being reported, the literature for mass-based penetration of CNTs through FFRs is lacking. The aim of this study was to conduct a quantitative study of single-walled CNT (SWCNT) and multiwalled CNT (MWCNT) penetration through FFRs. A CNT aerosol respirator testing system was used to generate charge-neutralized airborne SWCNTs and MWCNTs for this study. The size distribution was 20–10 000 nm, with 99% of the particles between 25 and 2840 nm. Mass median diameters were 598 and 634 nm with geometric standard deviations of 1.34 and 1.48 for SWCNTs and MWCNTs, respectively. Upstream and downstream CNTs were collected simultaneously using closed-face 3.7-cm-diameter filter cassettes. These samples were subsequently analyzed for organic carbon and elemental carbon (EC), with EC as a measure of mass-based CNTs. The mass-based penetration of SWCNTs and MWCNTs through six FFR models at constant flow rates of 30 l min^{-1} (LPM) was determined. Generally, the penetrations of SWCNTs and MWCNTs at 30 LPM had a similar trend and were highest for the N95 FFRs, followed by N99 and P100 FFRs. The mass-based penetration of MWCNTs through six FFR models at two constant flow rates of 30 and 85 LPM was also determined. The penetration of MWCNTs at 85 LPM was greater compared with the values of MWCNTs at 30 LPM.

KEYWORDS: aerosol respirator testing system; elemental carbon; filtering facepiece respirators; mass-based penetration; multiwalled carbon nanotubes; single-walled carbon nanotubes

INTRODUCTION

Carbon nanotubes (CNTs) are currently used in numerous industrial and biomedical applications, including electron field emitters, conductive plastics, semiconductor devices (Endo *et al.*, 2008; Wang *et al.*, 2011), chemical sensors and catalysts (McKinney *et al.*, 2009), biosensors, and medical devices (Chakravarty *et al.*, 2008; Endo *et al.*, 2008).

Several studies in rodents have shown: (i) acute pulmonary inflammation and interstitial fibrosis observed in CNT-exposed animals in subchronic studies (Shvedova *et al.*, 2008; Porter *et al.*, 2010) and (ii) an equal or greater potency of CNTs compared with other inhaled particles known to be hazardous to exposed workers (crystalline silica and asbestos) in causing adverse lung effects (Muller *et al.*, 2005; Shvedova *et al.*, 2005). Animal toxicological evidence suggests that a wide range of human health effects could result from exposure to CNTs [Poland *et al.*, 2008; National Institute for Occupational Safety and Health (NIOSH), 2013]. The toxicities may vary between the differing types of CNTs [single-walled CNTs (SWCNTs) or multiwalled CNTs (MWCNTs)] and the varying individual characteristics, such as raw versus purified forms, agglomerated structure versus single fibers, and fiber length (Donaldson *et al.*, 2006).

In general, SWCNTs range from 1 to 10 nm in diameters and have a strong tendency to form highly entangled structures with a nest-like appearance (Shvedova *et al.*, 2005; Maynard *et al.*, 2007), while MWCNTs possess diameters up to 100 nm with hollow cores and typically have bundled fibrous morphologies (Wang *et al.*, 2007). Due to the fibrous geometry and van der Waals forces, CNTs tend to form large agglomerates (bulk powder); therefore, the dispersion of these airborne particles with a controlled degree of agglomeration plays a significant role in CNT studies. We have recently developed a CNT aerosol generator to produce a sufficient amount of airborne CNTs with a controlled degree of agglomeration for testing of FFRs (Vo and Zhuang, 2013).

Studies have suggested that workers may be at risk for exposure to CNT particles during the manufacture, handling, and cleanup of CNT materials (Mitchell *et al.*, 2007; Evans *et al.*, 2010; Porter *et al.*, 2010; Birch *et al.*, 2011; Dahm *et al.*, 2012, 2013). With a concern for worker exposure to CNTs, several CNT exposure limits have been proposed. An interim occupational exposure limit of 21 μg m^{-3} for MWCNTs was proposed in a report by the Japanese New Energy and Industrial Technology Development Organization (Kobayashi *et al.*, 2009). NIOSH has also proposed a respirable mass-based recommended exposure limit (REL) for CNTs, with a REL of 7 μg m^{-3} as an 8-h time-weighted average (NIOSH, 2006, 2013). Inhalation of aerosolized CNT particles is believed to be the primary route of exposure and is of most concern (Evans *et al.*, 2010; Birch *et al.*, 2011; Dahm et al., 2012, 2013). A NIOSH survey of the carbonaceous nanomaterial industry found that 77% of the companies used some types of respiratory protection, such as N95 FFRs (Dahm *et al.*, 2011). Additionally, the NIOSH Current Intelligence Bulletin 65 (NIOSH, 2013) on CNTs and carbon nanofibers recommend workers to select and use respirators when working with nanoparticles. Thus, there is a need for mass-based FFR penetration data on CNTs.

The Scanning Mobility Particle Sizer (SMPS) and Aerodynamic Particle Sizer (APS) are commonly used to determine particle concentrations and size distributions of spheres and not applicable for elongated particles. Therefore, using an SMPS or APS to determine the mass-based penetration for longer CNT structures and CNT agglomerates may contribute to its underestimation due to their nonspherical form and the estimated values of CNT density and particle diameters. Recently, some mass-based, quantitative studies at facilities that manufacture and process CNTs (or nanofibers) have been conducted by collecting workplace air samples for subsequent analysis using the NIOSH Method 5040 (NIOSH, 2006, 2013) and/or electron microscopy (Maynard *et al.*, 2004; Methner *et al.*, 2007; Evans *et al.*, 2010; Lee *et al.*, 2010; Birch *et al.*, 2011; Dahm *et al.*, 2012); however, reports on the mass-based data of airborne CNT penetration through FFRs are lacking.

Although numerous respirator filtration studies have been done with surrogate engineered nanoparticles, such as sodium chloride, these studies used solvents as aerosol generator fluids (suspension solutions), were targeted toward generating spherical particles, and measured particles in the range of 100–400 nm mobility diameters (Wilkes, 2002; Rengasamy *et al.*, 2009). Thus, there is a need for a quantitative study on elongated-shape CNTs to determine CNT penetration through FFRs or other

respirator filters and to support the current NIOSH respirator recommendations.

The aims of this study were to generate airborne SWCNT and MWCNT particles continuously in a sufficient amount for testing of FFRs, with CNT size distributions in the respirable size range (particles < 10 μm), and to conduct a quantitative study of SWCNT and MWCNT penetration through FFRs using a thermal–optical analysis technique (Birch and Cary, 1996; NIOSH, 2006) for CNT measurement.

MATERIALS AND METHODS

Equipment and supplies

CNT aerosol respirator testing system

A CNT aerosol respirator testing system (CNT-ARTS) has been previously developed (Vo and Zhuang, 2013) and was used to generate a sufficient amount of airborne CNT particles in the respirable size range (particles < 10 μm) for testing of FFRs. The testing system was able to aerosolize airborne CNTs from bulk powder materials (Vo and Zhuang, 2013), rather than nebulizer dispersion of CNTs in a liquid suspension. Bulk powder dispersion is preferable because it is more representative of workplace dispersion during handling of CNT powders (Calvert *et al.*, 2009).

SWCNT and MWCNT samples

The SWCNT and MWCNT bulk materials used in this study were obtained from Nanostructured & Amorphous Materials, Inc. (SWNT-1246YJS, lot 1227-090111 and MWNT-1227YJS, lot 1227-041709; Houston, TX, USA) and used without further purification. According to the manufacturer, the average diameter of the SWCNTs is between 1 and 2 nm, while the length (geometric length) varies from 1 to 3 μm. The average diameter of the MWCNT product is between 30 and 80 nm, while the length varies from 0.5 to 2 μm.

Respirators

Two models of each N95, N99, and P100 series (total of six FFR models) were randomly selected from among those models tested previously in our laboratory (Vo and Shaffer, 2012). These FFR models were randomly assigned labels A or B for each series FFR models (Tables 1–3). Although elastomeric half-mask respirators (EHRs) and FFRs are commonly used by workers in the carbonaceous nanomaterial industry (Dahm *et al.*, 2011), the CNT contamination in the EHRs is of concern for this quantitative analysis study because the half-masks have to be reused while the FFRs are designed as 'single-use' devices; thus, the NIOSH-approved FFRs were selected for this study. These FFRs have a multilayer structure, and the main layers of these FFRs are composed of polypropylene fibers with electrical charge; however, each FFR model has different characteristics, such as number of layers, thickness, and different fiber materials.

Generation and characterization of airborne SWCNTs and MWCNTs

Generation of airborne SWCNTs and MWCNTs

Airborne SWCNTs and MWCNTs in the respirable size range (particles < 10 μm) were generated according to the method of Vo and Zhuang (2013). During generator operation, 1.0 g of bulk CNTs (SWCNTs or MWCNTs) and a small stir bar were placed inside the nebulizer cylinder (Fig. 1). Once the head form with the FFR was set up, the chamber was sealed and internal fans were started. Then, compressed air valves were opened and particles were aerosolized. The micro-stir bar was used to agitate the CNT samples and disperse them from the bulk powder. The flow of air at 7 l min^{-1} (LPM) through the nebulizer was used to carry small CNT particles out of the nebulizer cylinder, while larger particles tended to stay in the lower portion of the cylinder until they were dispersed. The CNT particles passed through a cyclone to establish the size cut-off particles ≥ 10 μm before they were directly mixed with clean dry air to reach a final designated CNT concentration (Fig. 1). Then, the airborne CNTs passed through a diffusion dryer to remove any associated water vapor. Before entering the exposure chamber, the airborne CNTs passed through a Kr-85 neutralizer. A Condensation Particle Counter (CPC, model 3776; TSI Inc., Shoreview, MN, USA) with a controlled flow rate of 1.5 LPM was used to monitor the CNT concentration in the chamber during particle generation (Fig. 1).

Characterization of airborne SWCNTs and MWCNTs

To investigate a constant output concentration, the CPC was used to monitor the CNTs in the chamber during particle generation. The CPC was also used to measure the CNT concentration to ensure that the

Table 1. EC results of upstream and downstream SWCNTs at constant flow rate of 30 LPM

FFR models	CNT sample	Sampling time (min)	Flow rate (LPM)	Mean EC[a] of SWCNTs on filter (μg)[b]	SWCNT concentration (μg l^{-1})[c]	SWCNT penetration (%)
N95-A	Upstream[d]	6	0.5	176.87 ± 21.15	58.96 ± 7.05	0.93 ± 0.28
	Downstream	80	3.0	134.30 ± 4.11	0.55 ± 0.02	
N95-B	Upstream[d]	6	0.5	176.87 ± 21.15	58.96 ± 7.05	0.47 ± 0.14
	Downstream	80	3.0	66.22 ± 2.01	0.28 ± 0.01	
N99-A	Upstream[d]	6	0.5	215.78 ± 25.80	71.93 ± 8.60	0.40 ± 0.12
	Downstream	90	3.0	77.97 ± 4.45	0.29 ± 0.01	
N99-B	Upstream[d]	6	0.5	215.78 ± 25.80	71.93 ± 8.60	0.38 ± 0.11
	Downstream	90	3.0	73.86 ± 4.02	0.27 ± 0.01	
P100-A	Upstream[d]	6	0.5	422.71 ± 50.55	140.90 ± 16.85	0.014 ± 0.005
	Downstream	200	3.0	9.59 ± 0.54	0.02 ± 0.001	
P100-B	Upstream[d]	6	0.5	422.71 ± 50.55	140.90 ± 16.85	0.007 ± 0.005
	Downstream	200	3.0	3.04 ± 0.32	0.01 ± 0.001	

[a]Mean EC ± RSD ($n = 3$): EC on the 3.7-cm-diameter filter.
[b]EC results calculated as: [EC (μg cm^{-2}) of the 1.5-cm^2 sample portion – EC of the control] × total deposit area of the 3.7-cm-diameter filter.
[c]SWCNT concentration: EC results on filter per liter of sampling air penetrated through the filter.
[d]Upstream: EC upstream values were averaged values for each FFR series type.

CNT-ARTS generated a sufficient amount of CNTs for testing of FFRs (≥3×10^4 particles per cm^3 required for P100-FFR) (Vo and Zhuang, 2013).

The size distribution of output SWCNTs and MWCNTs was measured using an APS and an SMPS as described by Vo and Zhuang (2013). The combination of the SMPS and APS data into a single size distribution (0.02–20 μm) was performed according to the method of Khlystov *et al.* (2004) by calculating the ratio of the overlapping size range between 0.6 and 0.9 μm.

SWCNT and MWCNT penetration through FFRs and quantitative analysis

The CNT penetration procedure

Before each penetration experiment, a FFR was sealed with silicone to the face of the head form and a leakage test was conducted using a breathing system as described by Vo and Zhuang (2013).

The penetration experiments were carried out using the penetration measurement system (Vo and Zhuang, 2013) at two constant flow rates: 30 LPM (which simulates inhalation at a normal work rate [Clayton *et al.*, 2002]) and 85 LPM (which simulates inhalation at a heavy work rate [Clayton *et al.*, 2002]). Airborne CNTs outside each FFR (near the center of the FFR, Fig. 1) were designated as upstream particles, and airborne CNTs that penetrated through each FFR (inside a head form, Fig. 1) were designated as downstream particles. The upstream and downstream samples were collected simultaneously, so the filter performance of all FFRs sealed with silicone to the face of the head form depended only on the ratio of the downstream and upstream particle concentrations. In addition, due to the high cost and high toxicity level of CNTs, minimal amounts of CNT samples were considered; therefore, different CNT concentrations in the chamber were generated for different P100 FFR series.

Collection of upstream and downstream CNT samples

In this study, all samples of SWCNTs and MWCNTs were collected using closed-face 3.7-cm-diameter filter cassettes (three-piece preloaded cassettes containing

Table 2. EC results of upstream and downstream MWCNTs at constant flow rate of 30 LPM

FFR models	CNT sample	Sampling time (min)	Flow rate (LPM)	Mean EC[a] of MWCNTs on filter (μg)[b]	MWCNT concentration (μg l^{-1})[c]	MWCNT penetration (%)
N95-A	Upstream[d]	6	0.5	198.87 ± 30.49	66.29 ± 10.16	0.83 ± 0.30
	Downstream	80	3.0	133.08 ± 8.63	0.55 ± 0.03	
N95-B	Upstream[d]	6	0.5	198.87 ± 30.49	66.29 ± 10.16	0.45 ± 0.20
	Downstream	80	3.0	72.70 ± 4.44	0.30 ± 0.02	
N99-A	Upstream[d]	6	0.5	342.87 ± 52.57	114.29 ± 17.52	0.18 ± 0.06
	Downstream	90	3.0	57.23 ± 1.84	0.21 ± 0.01	
N99-B	Upstream[d]	6	0.5	342.87 ± 52.57	114.29 ± 17.52	0.17 ± 0.06
	Downstream	90	3.0	55.25 ± 1.80	0.20 ± 0.01	
P100-A	Upstream[d]	6	0.5	445.31 ± 68.28	148.44 ± 22.76	0.013 ± 0.004
	Downstream	200	3.0	15.53 ± 0.34	0.02 ± 0.001	
P100-B	Upstream[d]	6	0.5	445.31 ± 68.28	148.44 ± 22.76	0.007 ± 0.004
	Downstream	200	3.0	6.86 ± 0.13	0.01 ± 0.001	

[a]Mean EC ± RSD (n = 3).
[b]EC results calculated as: (EC of the sample portion – EC of the control) × the total deposit area.
[c]MWCNT concentration: EC results on filter per liter of sampling air penetrated through the filter.
[d]Upstream: the EC upstream values were averaged values for each FFR series type.

3.7-cm-diameter quartz-fiber filters, model #: 225-401; SKC Inc., Eighty Four, PA, USA). For each FFR model, each set of three upstream and three downstream CNT samples were collected simultaneously on the quartz-fiber filters for organic carbon (OC) and elemental carbon (EC) analysis. Quartz-fiber filters were used because of their high collection efficiency for particulate matter and resistance to the high temperature (≥850°C) generated during the OC–EC analysis. The upstream CNTs were collected using an in-house vacuum system, including a 90-cm probe connected to the filter cassette, a mass flow meter (model #4140, TSI), and an air regulator to control the air flow rate (Fig. 1, 2 A–2C).

In order to obtain an even sample deposition across the filter and proper filter loadings, the sample collection conditions were designed as: (i) an airflow to the quartz-filter cassette ≤3 LPM and (ii) a filter loading level for both upstream and downstream samples <100 μg cm^{-2}. To achieve the sample collection requirements within the normal work period (≤4 h), different flow rates and sampling times for upstream and downstream samples were used as follows. The airflow to the filter cassette was set to 0.5 LPM for the upstream CNT samples. The collection time of the upstream CNT samples is shown in Tables 1–3. The downstream CNTs were collected using the same in-house vacuum connected to another 90-cm probe and mass flow meter (model #4140, TSI) (Fig. 1, 3A–3C). The airflow to the filter was set to 3 LPM for the downstream CNT samples. The collection time of the downstream CNT samples is also shown in Tables 1–3. After completing collection for each sample, the filter cassette was covered with the cassette cap and stored at room temperature prior to subsequent analysis to determine the mass-based CNT concentration, with EC used as a measure of CNT mass.

Quantitative analysis of CNTs using a thermal–optical technique

SWCNTs and MWCNTs collected on quartz-fiber filters were analyzed for OC and EC by NIOSH Method 5040, based on a thermal–optical analysis technique (Birch and Cary, 1996; Birch 2012; Chai *et al.* 2012).

Table 3. EC results of upstream and downstream MWCNTs at constant flow rate of 85 LPM

FFR models	CNT sample	Sampling time (min)	Flow rate (LPM)	Mean EC[a] of MWCNTs on filter (μg)[b]	MWCNT concentration (μg l^{-1})[c]	MWCNT penetration (%)
N95-A	Upstream[d]	3	0.5	116.31 ± 16.15	77.54 ± 9.77	1.08 ± 0.37
	Downstream	40	3.0	101.26 ± 4.80	0.84 ± 0.04	
N95-B	Upstream[d]	3	0.5	116.31 ± 16.15	77.54 ± 9.77	0.61 ± 0.18
	Downstream	80	3.0	113.62 ± 4.79	0.47 ± 0.02	
N99-A	Upstream[d]	3	0.5	151.20 ± 19.56	100.80 ± 13.04	0.26 ± 0.07
	Downstream	90	3.0	69.42 ± 5.38	0.26 ± 0.01	
N99-B	Upstream[d]	3	0.5	151.20 ± 19.56	100.80 ± 13.04	0.24 ± 0.07
	Downstream	90	3.0	63.75 ± 5.41	0.24 ± 0.01	
P100-A	Upstream[d]	3	0.5	302.41 ± 10.44	201.60 ± 6.96	0.025 ± 0.014
	Downstream	200	3.0	32.70 ± 0.37	0.05 ± 0.001	
P100-B	Upstream[d]	3	0.5	302.41 ± 10.44	201.60 ± 6.96	0.02 ± 0.014
	Downstream	200	3.0	23.20 ± 0.10	0.04 ± 0.001	

[a]Mean EC ± RSD (n = 3).
[b]EC results calculated as: (EC of the sample portion − EC of the control) × the total deposit area.
[c]MWCNT concentration: EC results on filter per liter of sampling air penetrated through the filter.
[d]Upstream: the EC upstream values were averaged values for each FFR series type.

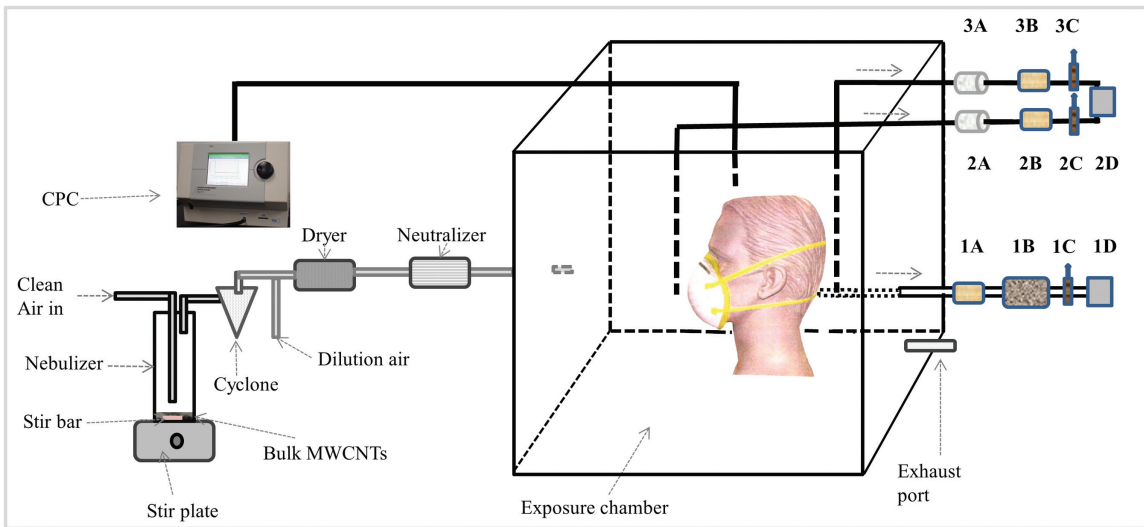

1 Schematic diagram of CNT aerosol respirator penetration system: including a constant air flow apparatus (mass flow meter, 1A; high efficiency particulate air (HEPA) filter, 1B; air regulator, 1C; in-house vacuum, 1D), upstream sample collection apparatus (closed-face sample cassette, 2A; mass flow meter, 2B; air regulator, 2C; in-house vacuum, 2D), and downstream sample collection apparatus (closed-face sample cassette, 3A; mass flow meter, 3B; air regulator, 3C; in-house vacuum, 2D).

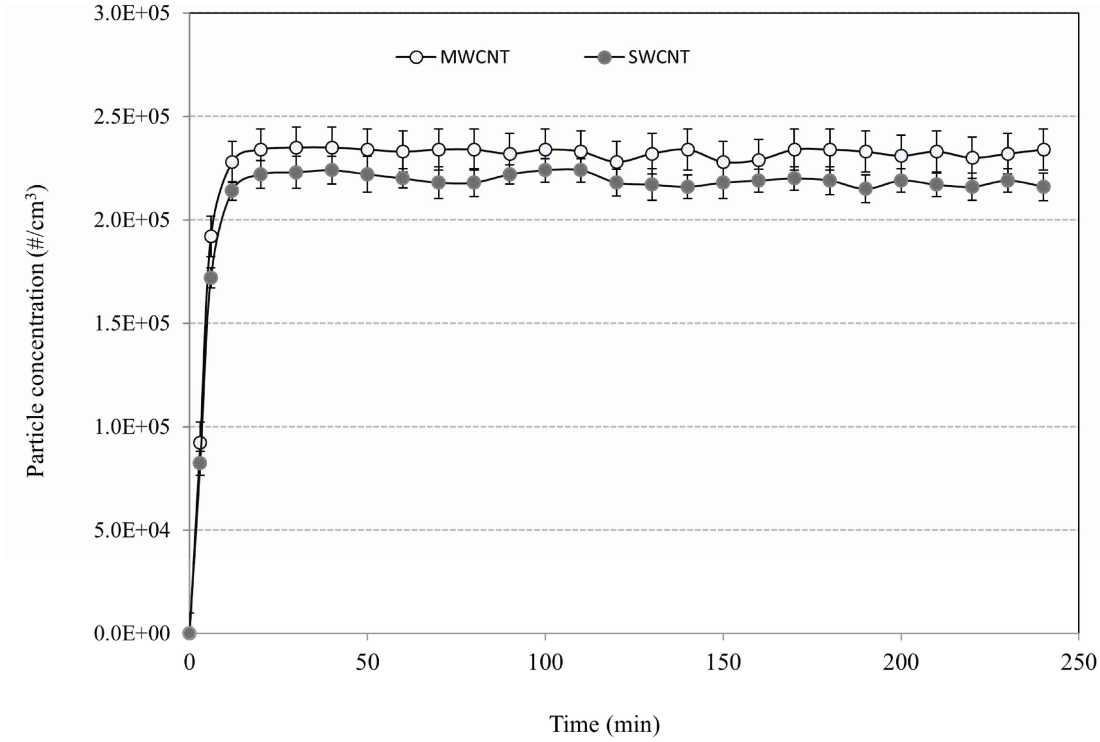

2 Average SWCNT and MWCNT concentrations ($n = 3$) at the center of the exposure chamber during a 4-h test period.

For each analysis, a portion (~1.5-cm^2 rectangular punch) of the filter sample was removed and inserted into the analyzer oven. The analysis proceeds in inert and oxidizing atmospheres. In both, evolved carbon is catalytically oxidized to carbon dioxide (CO_2) and the CO_2 is reduced to methane (CH_4), which is detected by a flame ionization detector. In the analysis, the temperature is first stepped in helium, to a preset maximum, to remove OC. If char forms as the sample is heated, the filter transmittance decreases with increasing temperature. After the OC is removed, an oxygen–helium mix is introduced and the temperature is again increased stepwise, to 850°C or higher (up to 920°C, depending on the sample), to oxidize the remaining material. As light-absorbing carbon (including any char formed) is oxidized, the filter transmittance increases. The OC–EC split is assigned when the initial transmittance value is reached. Carbon removed prior to the split is quantified as OC, while that removed after the split is quantified as EC. As mentioned, in this work, the automatic OC–EC split correction for pyrolysis was not necessary because the CNT material was composed of EC (i.e. there was no OC pyrolysis). Thus, the OC–EC split was set at a fixed time such that all the carbon removed during the second part of the analysis (in oxidizing atmosphere) was quantified as EC.

With each sample set analyzed, a sucrose solution was used as an external calibration standard. Additionally, a fixed volume of methane was automatically injected at the end of each analysis as an internal standard. As control samples, media blanks were also analyzed. As with the samples, a portion (~1.5-cm^2 punch) of the quartz filter media (as received in a sealed package) was removed and analyzed for the blank determinations.

For the respirator tests, airborne CNT samples were collected in an enclosed chamber with filtered air and (based on analysis of bulk materials) their OC content was negligible, so the CNT mass concentration was based only on the EC result. Based on the even sample deposition across the filter, a 1.5-cm^2 sample portion from each quartz filter was analyzed and representative of the entire deposit. Therefore, the total EC on the

filter was calculated as: [EC (μg cm^{-2}) on the 1.5-cm^2 sample portion – EC blank] × the total deposit area.

Mass-based CNT penetration

The mass-based SWCNT and MWCNT penetrations were calculated as a ratio of the downstream and upstream mass-based concentrations:

$$P = (C_{down}/C_{up}) \times 100$$

where C_{down} is the downstream mass-based concentration (total EC on the 3.7-cm-diameter filter per liter of downstream air containing CNT; μg l^{-1}); C_{up} is the upstream mass-based concentration (total EC on the filter per liter of upstream air containing CNT).

Data analysis

All tests in this study were replicated three times. The mean, standard deviation, and normal data distribution were calculated using Microsoft Excel 2010 software (Microsoft Corporation, Redmond, WA, USA). *P*-values of <0.05 were considered significant. To compare the percent penetration of SWCNT and MWCNT particles through each FFR model, paired *t*-tests with two-tailed distribution were run, also using Microsoft Excel 2010.

RESULTS

Characterization of airborne SWCNTs and MWCNTs

Results from our previous study using the SMPS and APS to investigate the size distribution (mobility equivalent diameter) of airborne CNTs in the testing chamber under the same test conditions showed the CNT size distribution was in the respirable size range (particles < 10 μm diameter) (Vo and Zhuang, 2013). The average size distribution was 20–10 000 nm, with 99% of the particles between 25 and 2840 nm, and mass median diameters were 598 and 634 nm with geometric standard deviations of 1.34 and 1.48 for output SWCNTs and MWCNTs, respectively.

In this study, the average output SWCNT and MWCNT concentrations during a 4-h test period were characterized using the CPC and found to be 2.19×10^5 ($\pm 2.79 \times 10^3$) and 2.32×10^5 ($\pm 2.33 \times 10^3$) particles per cm^3 for SWCNTs and MWCNTs, respectively ($n = 3$; Fig. 2).

Quantitative analysis of SWCNTs and MWCNTs

All upstream and downstream samples of SWCNTs at 30 LPM flow rate and MWCNTs at 30 and 85 LPM flow rates were collected for mass concentration analysis. All upstream and downstream samples of SWCNTs and MWCNTs were found to deposit evenly across the filter. Thus, a single punch (a 1.5-cm^2 sample portion) from each quartz filter was analyzed for EC and representative of the entire deposit. Results for SWCNT and MWCNT samples (corrected for media blank) are presented in Tables 1–3.

For SWCNT samples collected at 30 LPM, the total EC loadings for upstream samples ranged from 16.46 to 39.33 μg cm^{-2}. These loadings represent a concentration range from 58.96 to 140.90 μg l^{-1} per each filter (the 3.7-cm-diameter filter) for upstream samples, with a relative standard deviation (RSD) range of 7.05–16.85 ($n = 3$) for all six FFR models (Table 1). The EC loadings for downstream samples ranged from 0.28 to 12.50 μg cm^{-2}, which represents 0.01–0.55 μg l^{-1} for downstream concentrations, with RSD in the range of 0.001–0.02 ($n = 3$) for all FFR models (Table 1).

The EC loadings for upstream samples of MWCNTs collected at 30 LPM ranged from 18.50 to 41.43 μg cm^{-2}. This EC range represents 66.29–148.44 μg l^{-1} per each filter for upstream concentrations, with RSD in the range of 10.16–22.76 ($n = 3$) for all six FFR models (Table 2). The EC loadings for downstream samples ranged from 0.64 to 12.38 μg cm^{-2}, corresponding to 0.01–0.55 μg l^{-1} and a RSD in the range from 0.001 to 0.03 ($n = 3$) for all FFR models (Table 2).

The EC for upstream samples of MWCNTs collected at 85 LPM flow rate ranged from 10.82 to 28.14 μg cm^{-2}. These loadings represent 77.54–201.60 μg l^{-1} per each filter, with RSD in the range of 6.96–13.04 ($n = 3$) for all six FFR models (Table 3). The EC for downstream samples ranged from 2.16 to 10.82 μg cm^{-2}, corresponding to 0.04–0.84 μg l^{-1} for downstream mass-based concentrations, with RSD in the range of 0.001–0.04 ($n = 3$) for all FFR models (Table 3).

SWCNT and MWCNT penetrations

The percent mass-based penetration values of SWCNTs and MWCNTs for the six FFR models at a constant flow rate of 30 LPM are shown in Tables 1 and 2, respectively. Percent mass-based penetrations

of SWCNTs were highest for the N95 (0.47–0.93%), followed by N99 (0.38–0.40%) and P100 (0.007–0.014%) FFRs. For MWCNTs collected at 30 LPM, percent mass-based penetrations were also highest for the N95 (0.45–0.83%), followed by N99 (0.17–0.18%) and P100 (0.007–0.013%) FFRs. The paired *t*-tests ran for the N95-A and N95-B models revealed *P*-values of 0.006 and 0.003 for SWCNTs and MWCNTs at the flow rate of 30 LPM, respectively. This indicates that penetrations were significantly different between the N95-A and N95-B models; however, penetrations were not significantly different between the N99-A and N99-B (all *P*-values > 0.2) or the P100-A and P100-B models (all *P*-values > 0.07) for both SWCNT and MWCNT experiments. The results in Table 1 also show that the SWCNT penetration of the N95-B approached the performance of the N99-A and N99-B models with all *P*-values > 0.2.

The percent mass-based penetration values of MWCNTs for the six FFR models at constant flow rates of 30 and 85 LPM are shown in Tables 2 and 3, respectively. The results indicate that the percent mass-based penetrations at 85 LPM (0.61–1.08% for N95, 0.24–0.26% for N99, and 0.02–0.025% for P100 FFRs) were consistently greater compared with the values at 30 LPM (0.45–0.83% for N95, 0.17–0.18% for N99, and 0.007–0.013% for P100 FFRs) for all FFR models with all *P*-values < 0.03.

DISCUSSION

The results from this study show that the CNT-ARTS was capable of generating a sufficient amount of airborne SWCNTs and MWCNTs for testing of FFRs and able to maintain a stable CNT concentration during a 4-h test period.

In general, N95 FFRs allow higher levels of mass-based penetration compared with N99 or P100 FFRs for both SWCNTs and MWCNTs at the same constant flow rate of 30 LPM (all *P*-values < 0.01). The mass-based penetrations for SWCNTs were greater compared with the values for MWCNTs for all N95 and N99 FFR models (all *P*-values < 0.03). Two possible explanations for the larger SWCNT penetration for N95 and N99 FFRs are: (i) the output SWCNTs have smaller particle diameters with a mass median diameter (MMD) of 598 nm than the particle diameters of MWCNTs (MMD = 634 nm) and (ii) the increasingly hydrophilic fiber materials in each layer of N95 and N99 FFR series might contribute to this penetration trend (Rengasamy *et al.*, 2013). However, the penetrations for SWCNTs were not significantly different compared with the values for MWCNTs for P100 FFR models (all *P*-values ≥ 0.05). A possible reason for the similar penetrations could be that all P100 FFR models have the same number of filter layers and hydrophilic/hydrophobic layer characteristics (Rengasamy *et al.*, 2013).

For different FFR models within each FFR series, the results show that the mass-based penetrations of SWCNTs and MWCNTs at 30 LPM were significantly different between the N95-A (0.83–0.93%) and the N95-B (0.45–0.47%) models with all *P*-values ≤ 0.006. A possible explanation for the different penetrations is that the N95-A FFR model has a hydrophilic outer layer, while the N95-B FFR model has a hydrophobic outer layer (Rengasamy *et al.*, 2013). However, penetrations were not significantly different between the N99-A and N99-B or P100-A and P100-B models (all *P*-values > 0.07). A possible explanation for insignificantly different penetrations is that both the N99-A and N99-B or the P100-A and P100-B models have the same number of filter layers and hydrophilic/hydrophobic layer characteristics (Rengasamy *et al.*, 2013).

Comparison of the mass-based penetrations of MWCNTs at two different flow rates of 30 and 85 LPM indicated that different FFR models yielded different mass-based MWCNT penetrations (all *P*-values < 0.03), with larger penetrations observed for each model at the higher flow rate. Mass-based penetrations of MWCNTs for both 30 and 85 LPM experiments had a similar trend in the penetration and were highest for the N95 FFRs, followed by N99 and P100 FFRs. The different filter properties (hydrophilic/hydrophobic fiber materials and electrical charges), numbers of filter layers, and total filter thickness among the three different FFR series (N95, N99, and P100) would contribute to this penetration trend (Rengasamy *et al.*, 2013).

The principal limitation of this study is that the FFRs were sealed to the face of the head form, so their efficiency determined during experiments was defined as the efficiency of the FFR filter material. The actual field-measured penetration may be higher if there is some leakage between the wearer's face and the FFR. It should be noted that these test aerosols were

charge-neutralized particles and no moisture collection was present on the filter media in this study, so the actual field-measured penetration may be different. In addition, only limited FFR models were tested and other models may perform better or worse than those selected.

CONCLUSIONS

The mass-based penetration of SWCNTs and MWCNTs through six FFR models was determined by collection of samples on quartz-fiber filters and subsequent analysis using a thermal–optical technique. The results show that N95 FFRs allow higher levels of penetration compared with N99 or P100 FFRs, for both SWCNTs and MWCNTs at the same constant flow rate of 30 LPM. The results also show that the mass-based penetration of MWCNTs at 85 LPM flow rate was greater compared with the values at 30 LPM. As expected for dispersed powder aerosols with particle agglomerates in the respirable size range, results indicate that the mass-based penetrations of MWCNTs (0.61–1.08% for N95, 0.24–0.26% for N99, and 0.02–0.025% for P100) were less than the acceptable penetrations of these FFR models (≤5% for N95, ≤1% for N99, and ≤0.03% for P100 FFRs) for a sphere of unit density with the same constant flow rate of 85 LPM.

ACKNOWLEDGEMENTS

The authors thank Dr Samy Rengasamy, Dr Ron Shaffer (NIOSH/NPPTL, Pittsburgh, PA), and Dr David Murray (NIOSH/NPPTL, Morgantown, WA) for their valuable review comments for the manuscript.

DISCLAIMER

The findings and conclusions in this manuscript are those of the authors and do not necessarily represent the views of the National Institute for Occupational Safety and Health (NIOSH). Mention of company names or products does not constitute endorsement by NIOSH.

REFERENCES

Birch ME. (2012) Current Intelligence Bulletin: occupational exposure to carbon nanotubes and nanofibers, NIOSH Docket Number: NIOSH 161-A. See Appendix C: NIOSH Method 5040 and exposure monitoring section. Available at www.cdc.gov/niosh/docket/review/docket161A. Accessed 4 October 2013.

Birch ME, Cary RA. (1996) Elemental carbon-based method for monitoring occupational exposures to particulate diesel exhaust. *Aerosol Sci Technol*; **25**: 221–41.

Birch ME, Ku BK, Evans DE *et al.* (2011) Exposure and emissions monitoring during carbon nanofiber production. Part I: elemental carbon and iron-soot aerosols. *Ann Occup Hyg*; **55**: 1016–36.

Calvert G, Ghadiri M, Tweedie R. (2009) Aerodynamic dispersion of cohesive powders: a review of understanding and technology. *Adv Powder Technol*; **20**: 4–16.

Chai M, Birch ME, Deye G. (2012) Organic and elemental carbon filter sets: preparation method and interlaboratory results. *Ann Occup Hyg*; **56**: 959–67.

Chakravarty P, Marches R, Zimmerman NS *et al.* (2008) Thermal ablation of tumor cells with antibody-functionalized single-walled carbon nanotubes. *Proc Natl Acad Sci USA*; **105**: 8697–702.

Clayton MP, Bancroft B, Rajan B. (2002) A review of assigned protection factors of various types and classes of respiratory protective equipment with reference to their measured breathing resistances. *Ann Occup Hyg*; **46**: 537–47.

Dahm MM, Evans DE, Schubauer-Berigan MK *et al.* (2012) Occupational exposure assessment in carbon nanotube and nanofiber primary and secondary manufacturers. *Ann Occup Hyg*; **56**: 542–56.

Dahm MM, Evans DE, Schubauer-Berigan MK *et al.* (2013) Occupational exposure assessment in carbon nanotube and nanofiber primary and secondary manufacturers: mobile direct-reading sampling. *Ann Occup Hyg*; **57**: 328–44.

Dahm M, Yencken M, Schubauer-Berigan M. (2011) Exposure control strategies in the carbonaceous nanomaterial industry. *J Occup Environ Med*; **53**: S68–73.

Donaldson K, Aitken R, Tran L *et al.* (2006) Carbon nanotubes: a review of their properties in relation to pulmonary toxicology and workplace safety. *Toxicol Sci*; **92**: 5–22.

Endo M, Strano MS, Ajayan PM. (2008) Potential applications of carbon nanotubes. *Carbon Nanotubes*; **111**: 13–61.

Evans DE, Ku BK, Birch ME *et al.* (2010) Aerosol monitoring during carbon nanofiber production: mobile direct-reading sampling. *Ann Occup Hyg*; **54**: 514–31.

Khlystov A, Stanier C, Pandis SN. (2004) An algorithm for combining electrical mobility and aerodynamic size distributions data when measuring ambient aerosol. *Aerosol Sci Technol*; **38**: 229–38.

Kobayashi N, Kishimoto A, Ogura I. (2009) Risk assessment of manufactured nanomaterials: carbon nanotubes (CNTs). In Nakanishi J, editor. *Interim report issued on October 16, 2009. Executive summary*. Available at http://www.cdc.gov/niosh/

docket/archive/pdfs/NIOSH-161-A/0161-A-101609-Nakanishi-Attach1.pdf (Pages 1–48). Accessed 4 October 2013.

Lee JH, Lee SB, Bae GN *et al.* (2010) Exposure assessment of carbon nanotube manufacturing workplaces. *Inhal Toxicol*; **22**: 369–81.

Maynard AD, Baron PA, Foley M *et al.* (2004) Exposure to carbon nanotube material: aerosol release during the handling of unrefined single walled carbon nanotube material. *J Toxicol Environ Health A*; **67**: 87–108.

Maynard AD, Ku BK, Emery M *et al.* (2007) Measuring particle size-dependent physiochemical structure in airborne single walled carbon nanotube agglomerates. *J Nanopart Res*; **9**: 85–92.

McKinney W, Chen BT, Frazer D. (2009) Computer controlled multi-walled carbon nanotube inhalation exposure system. *Inhal Toxicol*; **21**: 1053–61.

Methner MM, Birch ME, Evans DE *et al.* (2007) Case study: identification and characterization of potential sources of worker exposure to carbon nanofibers during polymer composite laboratory operations. *J Occup Environ Hyg*; **4**: 125–30.

Mitchell L, Gao J, Vander Wal R *et al.* (2007) Pulmonary and systemic immune response to inhaled multiwalled carbon nanotubes. *Toxicol Sci*; **100**: 203–14.

Muller J, Huaux F, Moreau N *et al.* (2005) Respiratory toxicity of multi-wall carbon nanotubes. *Toxicol Appl Pharmacol*; **207**: 221–31.

NIOSH (National Institute for Occupational Safety and Health). (2013) NIOSH Docket Number 161A. Current Intelligence Bulletin 65: occupational exposure to carbon nanotubes and nanofibers. Cincinnati, OH: Department of Health and Human Services, Public Health Service, Centers for Disease Control and Prevention,National Institute for Occupational Safety and Health. DHHS (NIOSH). Available at: http://www.cdc.gov/niosh/docket/archive/docket161A.html. Accessed 2 October 2013.

NIOSH Manual of Analytical Methods. (2006) Method 5040 diesel particulate matter (as elemental carbon). In Schlecht PC, O'Connor PF, editors. *NIOSH method of analytical methods*. 4th edn., Issue 1. Cincinnati, OH: Department of Health and Human Services, Public Health Service, Centers for Disease Control and Prevention, National Institute for Occupational Safety and Health. DHHS (NIOSH). Publication 94-113.

Poland CA, Duffin R, Kinloch I *et al.* (2008) Carbon nanotubes introduced into the abdominal cavity of mice show asbestos-like pathogenicity in a pilot study. *Nat Nanotechnol*; **7**: 423–8.

Porter DW, Hubbs AF, Mercer RR *et al.* (2010) Mouse pulmonary dose- and time course- responses induced by exposure to multi-walled carbon nanotubes. *Toxicologist*; **269**: 136–47.

Rengasamy S, Eimer B, Shaffer RE. (2009) Comparison of nanoparticle filtration performance of NIOSH-approved and CE marked iltering facepiece respirators. *Ann Occup Hyg*; **53**: 117–28.

Rengasamy S, Miller A, Vo E *et al.* (2013) Filter performance degradation of electrostatic N95 and P100 filtering facepiece respirators by dioctyl phthalate aerosol loading. *J Eng Fibers Fabrics*; **8**: 62–9.

Shvedova AA, Kisin ER, Mercer R *et al.* (2005) Unusual inflammatory and fibrogenic pulmonary responses to single walled carbon nanotubes in mice. *Am J Physiol Lung Cell Mol Physiol*; **289**: L698–708.

Shvedova AA, Kisin E, Murray AR *et al.* (2008) Inhalation vs. aspiration of single-walled carbon nanotubes in C57BL/6 mice: inflammation, fibrosis, oxidative stress, and mutagenesis. *Am J Physiol Lung Cell Mol Physiol*; **295**: L552–65.

Vo E, Shaffer R. (2012) Development and characterization of a new test system to challenge personal protective equipment with virus-containing particles. *J Int Soc Resp Protect*; **29**: 13–29.

Vo E, Zhuang Z. (2013) Development of a new test system to determine penetration of multi-walled carbon nanotubes through filtering facepiece respirators. *J Aerosol Sci* **61**: 50–9.

Wang H, Ming K, Hu X *et al.* (2007) Synthesis of aligned carbon nanotubes on double-sided metallic substrate by chemical vapor deposition. *J Phys Chem C*; **111**: 12617–24.

Wang J, Kim SC, Pui DYH. (2011) Measurement of multi-wall carbon nanotube penetration through a screen filter and single-fiber analysis. *J Nanopart Res*; **13**: 4565–73.

Wilkes AR. (2002) Comparison of two techniques for measuring penetration of sodium chloride particles through breathing system filters. *Br J Anaesth*; **89**: 541–5.